

# Mutual Interactions of Lamb Waves in Nonlinear Elastic Plates

Shuyi Ma <sup>1</sup>, Guixian Zhang <sup>1</sup>, Hongfeng Hou <sup>1,\*</sup> and Lidong Wang <sup>2</sup><sup>1</sup> School of Traffic and Electrical Engineering, Dalian University of Science and Technology, Dalian 116052, China<sup>2</sup> Dalian Shipbuilding Industry Co., Ltd., Dalian 110624, China

\* Correspondence: houhf@dlust.edu.cn

**Abstract:** The mutual interactions of Lamb waves in nonlinear elastic plates are studied in this article. Many researchers have investigated the interactions of Lamb wave modes at nonlinear higher harmonics. However, little is known about nonlinearity-driven Lamb modulations from two primary modes with different frequencies. In this study, the existence of symmetric or antisymmetric mode due to Lamb wave mutual interactions is firstly theoretically formulated. Then, an approach is proposed to evaluate the intensity of phase velocity matching for selecting primary modes. Finally, the characteristics of the modulated wave generation are investigated and demonstrated. The generation of modulated waves in an aluminum plate and fatigue crack can be detected by mutual interactions of Lamb waves. The main contribution of this work is the proposed mutual interaction theory of Lamb waves in fatigue plates, which can guide fatigue detection in the metal plate.

**Keywords:** Lamb waves; nonlinear; mutual interactions



**Citation:** Ma, S.; Zhang, G.; Hou, H.; Wang, L. Mutual Interactions of Lamb Waves in Nonlinear Elastic Plates. *Metals* **2022**, *12*, 2175. <https://doi.org/10.3390/met12122175>

Academic Editor: Varvara Romanova

Received: 1 November 2022

Accepted: 12 December 2022

Published: 16 December 2022

**Publisher's Note:** MDPI stays neutral with regard to jurisdictional claims in published maps and institutional affiliations.



**Copyright:** © 2022 by the authors. Licensee MDPI, Basel, Switzerland. This article is an open access article distributed under the terms and conditions of the Creative Commons Attribution (CC BY) license (<https://creativecommons.org/licenses/by/4.0/>).

## 1. Introduction

Recent research has demonstrated that nonlinear ultrasonic-guided waves have the capability to provide sensitivity to microstructural changes [1–10]. When incident Lamb waves propagate in a media with a nonlinear mechanism such as a fatigue crack, nonlinear components, including higher harmonics due to the primary mode self-interactions and modulations due to mutual interactions, are generated from the nonlinear region [11–14]. These nonlinear components can be directly attributed to the nonlinear elastic properties of a material, which are much more sensitive to the changes in microstructure than linear elastic properties.

Many researchers have investigated higher harmonic generation from the primary mode self-interactions [15–17]. Hong [18] investigated the nonlinear features extracted from Lamb wave signals, which were demonstrably sensitive to impact damage. Pineda [19] presented a theoretical development and experimental investigation into the nonlinear guided wave for bolted joint health monitoring. The effect of load cycle numbers in nonlinear guided wave features was investigated. Aseem [20] also studied the debonding detection and location estimation method by nonlinear longitudinal guided waves in rebar-reinforced concrete structures.

However, there has been little study of the mutual interactions of Lamb waves. Liu et al. studied the interactions of guided waves in weakly nonlinear circular cylinders and plates, but they only discussed the generation of the second harmonics mode [21]. Lim and Sohn et al. studied the binding condition of Lamb wave nonlinear modulation [22]. It was validated that a nonlinear modulation requires synchronism, nonzero power flux, and simultaneous arrival. Then a fatigue crack detection technology using nonlinear ultrasonic wave modulation was proposed by Sohn et al. [11,23,24]. Based on low-frequency S0 mode and A0-S0 Lamb wave mixing wave method, Ding [25] studied the early stage damage by experiment investigation. It was shown that the Lamb mixing wave method was practicable for detecting early-stage damage. Donatas [26] investigated the selection of higher order Lamb wave mode for pipeline damage detection and detected the hidden

corrosion defect. Kim [27] presented a nondestructive method for the quantitative assessment of fatigue damage by the nonlinear ultrasonic method. SAFE method and experiment investigation were carried out on the damaged SWO-V spring coil.

The contributions of this work are shown as follows:

- (1) As the characteristics of the nonlinear modulation are practically important for its applications, the mutual interactions of Lamb waves in nonlinear elastic plates are studied in this study;
- (2) The Lamb wave mutual interaction theory can be utilized to guide nonlinear mode selection;
- (3) The fatigue damage in the metal plate can be detected by the Lamb wave mutual interaction.

The remainder of this paper is organized as follows: First, the existence of symmetric or antisymmetric mode due to Lamb waves mutual interactions is theoretically formulated. Then an approach is proposed to evaluate the intensity of phase velocity matching for selecting primary modes. Next, the characteristics of the modulated wave generation are investigated and demonstrated. Finally, the experiment is carried out on a 3 mm thick 6061-T6 aluminum plate to test the theoretical result and prove the effectiveness of fatigue damage detection by mutual interaction.

## 2. Nonlinear Modulation Generation of Lamb Waves

### 2.1. Lamb Wave Propagation

The wave motion is assumed to take place in the  $x_1x_3$  plane with propagation in the  $x_1$  direction, as illustrated in Figure 1.

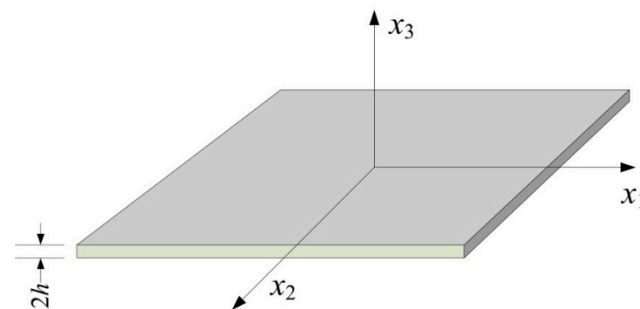


**Figure 1.** Free-plate schematic showing geometry.

For a given frequency, the displacement fields of the Lamb mode in the complex-value representation are given by [28].

$$\begin{aligned} u_1(x_1, x_3, t) &= (ikA \cos \alpha x_3 + \beta B \cos \beta x_3) e^{i(kx_1 - \omega t)} \\ u_3(x_1, x_3, t) &= (-\alpha A \sin \alpha x_3 - ikB \sin \beta x_3) e^{i(kx_1 - \omega t)} \end{aligned} \quad (1)$$

for the symmetric modes, where  $A$  and  $B$  are given as an eigenvector of

$$\begin{bmatrix} -2ik\alpha \sin \alpha h & (k^2 - \beta^2) \sin \beta h \\ (k^2 - \beta^2) \cos \beta h & -2ik\beta \cos \beta h \end{bmatrix} \begin{pmatrix} A \\ B \end{pmatrix} = \begin{pmatrix} 0 \\ 0 \end{pmatrix} \quad (2)$$

On the other hand, for the antisymmetric modes,

$$\begin{aligned} u_1(x_1, x_3, t) &= (ikC \sin \alpha x_3 - \beta D \sin \beta x_3) e^{i(kx_1 - \omega t)} \\ u_3(x_1, x_3, t) &= (\alpha C \cos \alpha x_3 - ikD \cos \beta x_3) e^{i(kx_1 - \omega t)} \end{aligned} \quad (3)$$

where  $C$  and  $D$  are given by [29]

$$\begin{bmatrix} 2ik\alpha \cos \beta h & (k^2 - \beta^2) \cos \beta h \\ (k^2 - \beta^2) \sin \alpha h & 2ik\beta \sin \beta h \end{bmatrix} \begin{pmatrix} C \\ D \end{pmatrix} = \begin{pmatrix} 0 \\ 0 \end{pmatrix} \tag{4}$$

Here,  $\omega$  and  $k$  are the angular frequency and the wave number of the Lamb mode, respectively. In addition,

$$\alpha = \sqrt{\left(\frac{\omega}{C_L}\right)^2 - k^2}, \beta = \sqrt{\left(\frac{\omega}{C_T}\right)^2 - k^2}. \tag{5}$$

$C_L$  and  $C_T$  are the longitudinal and transverse wave speeds, respectively,

$$c_L^2 = \frac{\lambda + 2\mu}{\rho}, c_T^2 = \frac{\mu}{\rho}$$

$\lambda, \mu$  are the Lamé parameters.

### 2.2. The Dispersion Property

Dispersion curves of the 3 mm isotropic aluminum plate are shown in Figure 2. The mass density ( $\rho$ ), Young’s modulus ( $E$ ), and Poisson’s ratio ( $\nu$ ) of the 3 mm isotropic aluminum plate are 2700 kg/m<sup>3</sup>, 71 GPa, and 0.33, respectively. As shown in Figure 2, with a frequency of under 520 kHz, there are only S0 and A0 modes. The investigation frequency is under 520 kHz.

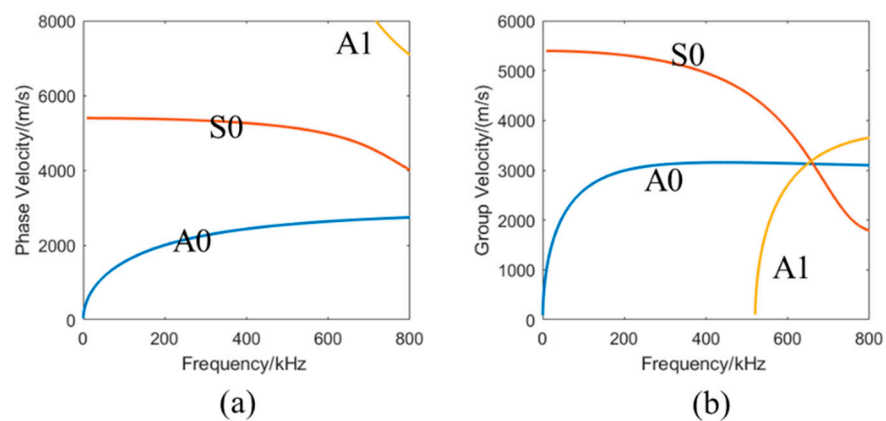


Figure 2. Dispersion curves of the 3 mm isotropic aluminum plate: (a) phase velocity; (b) group velocity.

### 2.3. Mutual Interaction

The wave motion is assumed to take place in a stress-free plate of thickness  $2h$  ( $x_3$  direction) with propagation in the  $x_1$  direction. Consider the interactions of two Lamb wave modes  $\mathbf{u}^a$  and  $\mathbf{u}^b$  propagating in the free plate. The total displacement field can be decomposed into fundamental and secondary wave fields

$$\mathbf{u} = \mathbf{u}^{(1)} + \mathbf{u}^{(2)}, \mathbf{u}^{(1)} = \mathbf{u}^a + \mathbf{u}^b, \mathbf{u}^{(2)} = \mathbf{u}^{aa} + \mathbf{u}^{bb} + \mathbf{u}^{ab}, \tag{6}$$

where  $\mathbf{u}^{aa}$  and  $\mathbf{u}^{bb}$  are the secondary wave fields due to the self-interactions of mode  $a$  and mode  $b$ , respectively, and  $\mathbf{u}^{ab}$  is the displacement field due to the mutual interactions of the two modes. The mode interaction problem can be solved by the normal mode expansion technique of Auld [30]. The secondary solution is written as

$$\mathbf{v}^{(2)}(x_1, x_3, t) = \frac{1}{2} \sum_{m=1}^{\infty} \frac{i(p_n^{surf} + p_n^{vol})}{4P_{mn}[k_n^* - (k_a \pm k_b)]} \mathbf{v}_m(x_3) \cdot \left( e^{i(k_a \pm k_b)x_1} - e^{ik_n^*x_1} \right) e^{-i(\omega_a \pm \omega_b)t} + c.c., k_n^* \neq (k_a \pm k_b), \tag{7}$$

$$\mathbf{v}^{(2)}(x_1, x_3, t) = \frac{1}{2} \sum_{m=1}^{\infty} \frac{x_1 (p_n^{surf} + p_n^{vol})}{4P_{mn}} \mathbf{v}_m(x_3) \cdot e^{i(k_a \pm k_b)x_1 - i(\omega_a \pm \omega_b)t} + c.c., k_n^* = (k_a \pm k_b), \quad (8)$$

where  $\mathbf{v}_m$  is the particle velocity of the  $m$ th secondary wave mode at  $\omega_a \pm \omega_b$ , and  $P_{mn}$  is the complex power flux in the propagation direction. For a propagating wave, the complex power flux exists only when  $m$  equals  $n$ . That is because mode  $n$  is orthogonal to all the other modes except itself, i.e.,  $P_{mn} \cdot p_n^{surf}$ , and  $p_n^{vol}$ , are interpreted as power fluxes through the surface and the volume, respectively [22], due to the nonlinear surface traction and body force exerted by the fundamental waves in the plates. Here,

$$P_{mn} = -\frac{1}{4} \int_{-h}^h (\mathbf{v}_n^* \cdot \mathbf{T}_m + \mathbf{v}_n \cdot \mathbf{T}_m^*) \cdot \mathbf{n}_1 dx_3, \quad (9)$$

$$p_n^{vol} = \frac{1}{2} \int_{-h}^h \mathbf{v}_n^* \cdot \mathbf{f} dx_3, \quad (10)$$

$$p_n^{surf} = -\frac{1}{2} \mathbf{v}_n^* \cdot \mathbf{T} \cdot \mathbf{n}_3 \Big|_{x_3=-h}^{x_3=h}, \quad (11)$$

where  $\mathbf{T}$  and  $\bar{\mathbf{T}}$  are the linear and nonlinear parts of the stress tensor for the mode mutual interactions, respectively, which can be obtained by [14]

$$T_{ij} = \lambda \frac{\partial u_k}{\partial x_k} \delta_{ij} + \mu \left( \frac{\partial u_j}{\partial x_i} + \frac{\partial u_i}{\partial x_j} \right) \quad (12)$$

$$\begin{aligned} \bar{T}_{ij} = & \frac{\lambda}{2} \frac{\partial u_k}{\partial x_i} \frac{\partial u_k}{\partial x_j} \delta_{ij} + (\lambda + B) \frac{\partial u_l}{\partial x_l} \frac{\partial u_j}{\partial x_i} + C \frac{\partial u_k}{\partial x_k} \frac{\partial u_l}{\partial x_l} \delta_{ij} \\ & + \frac{B}{2} \left( \frac{\partial u_k}{\partial x_j} \frac{\partial u_k}{\partial x_i} + \frac{\partial u_k}{\partial x_i} \frac{\partial u_l}{\partial x_k} \right) \delta_{ij} + B \left( \frac{\partial u_l}{\partial x_l} \frac{\partial u_i}{\partial x_j} \right) + \frac{A}{4} \frac{\partial u_i}{\partial x_k} \frac{\partial u_k}{\partial x_j} \\ & + \left( \mu + \frac{A}{4} \right) \left( \frac{\partial u_k}{\partial x_i} \frac{\partial u_j}{\partial x_k} + \frac{\partial u_i}{\partial x_k} \frac{\partial u_j}{\partial x_k} + \frac{\partial u_k}{\partial x_i} \frac{\partial u_k}{\partial x_j} \right) \end{aligned} \quad (13)$$

Finally, the nonlinear body force is given by the divergence of the nonlinear stress

$$\bar{\mathbf{f}} = \nabla \cdot \bar{\mathbf{T}}. \quad (14)$$

The quantities in Equation (13) are the real primary displacement field  $u_i$ ; Lamé's constant  $\lambda$ ; the shear modulus  $\mu$ ; and the third-order elastic material constants  $A$ ,  $B$ , and  $C$ .

The nonlinear forcing terms for mode mutual interaction problems can be obtained by substituting  $\mathbf{u}^a$  and  $\mathbf{u}^b$  into Equations (13) and (14) while retaining terms up to the second order for the nonlinear stress and the nonlinear body forces. Therefore, the nonlinear stress for the mode of mutual interactions is given by [14]

$$\begin{aligned} \bar{T}_{ij}^M = & (\lambda + B) \left( \frac{\partial u_k^a}{\partial x_k} \frac{\partial u_j^b}{\partial x_i} + \frac{\partial u_j^a}{\partial x_j} \frac{\partial u_i^b}{\partial x_l} \right) + \left( \lambda \frac{\partial u_l^a}{\partial x_k} \frac{\partial u_l^b}{\partial x_k} + 2C \frac{\partial u_k^a}{\partial x_k} \frac{\partial u_l^b}{\partial x_l} \right) \delta_{ij} \\ & + B \left( \frac{\partial u_k^a}{\partial x_k} \frac{\partial u_i^b}{\partial x_j} + \frac{\partial u_j^a}{\partial x_j} \frac{\partial u_l^b}{\partial x_l} \right) + \frac{B}{2} \left( \frac{\partial u_k^a}{\partial x_l} \frac{\partial u_k^b}{\partial x_l} + \frac{\partial u_l^a}{\partial x_k} \frac{\partial u_k^b}{\partial x_l} + \frac{\partial u_l^a}{\partial x_k} \frac{\partial u_l^b}{\partial x_k} + \frac{\partial u_l^a}{\partial x_k} \frac{\partial u_l^b}{\partial x_k} \right) \delta_{ij} \\ & + \left( \mu + \frac{A}{4} \right) \left( \frac{\partial u_k^a}{\partial x_i} \frac{\partial u_j^b}{\partial x_k} + \frac{\partial u_j^a}{\partial x_k} \frac{\partial u_k^b}{\partial x_i} + \frac{\partial u_i^a}{\partial x_k} \frac{\partial u_j^b}{\partial x_k} + \frac{\partial u_j^a}{\partial x_k} \frac{\partial u_i^b}{\partial x_k} + \frac{\partial u_k^a}{\partial x_i} \frac{\partial u_k^b}{\partial x_j} + \frac{\partial u_k^a}{\partial x_j} \frac{\partial u_k^b}{\partial x_i} \right) \\ & + \frac{A}{4} \left( \frac{\partial u_l^a}{\partial x_k} \frac{\partial u_k^b}{\partial x_j} + \frac{\partial u_k^a}{\partial x_j} \frac{\partial u_l^b}{\partial x_k} \right) + O \left( \left( \frac{\partial u_j^a}{\partial x_i} \right)^3 \right) + O \left( \left( \frac{\partial u_j^b}{\partial x_i} \right)^3 \right), \end{aligned} \quad (15)$$

and the nonlinear body force for the mode of mutual interaction is given by

$$\bar{f}_i^M = \sum_{j=1}^3 \frac{\partial \bar{T}_{ij}^M}{\partial x_j}. \quad (16)$$

Equations (15) and (16) give the nonlinear forcing terms for the mode of mutual interaction, and the result is shown in the Appendix A.

The matrix forms of the nonlinear forcing terms can be written in matrix form as

$$\mathbf{T}^{-M} = \begin{bmatrix} \bar{T}_{11}^M & 0 & \bar{T}_{13}^M \\ 0 & 0 & 0 \\ \bar{T}_{31}^M & 0 & \bar{T}_{33}^M \end{bmatrix} \quad (17)$$

$$\mathbf{f}^{-M} = \begin{Bmatrix} \bar{f}_1^M \\ 0 \\ \bar{f}_3^M \end{Bmatrix} \quad (18)$$

which enables the determination of the possible types of cumulative secondary wave fields due to guided wave mutual interactions with two Lamb modes.

With regards to Lamb mode secondary wave fields, the power flux from an arbitrary fundamental mode to a prescribed Lamb secondary mode via the nonlinear stress is given by

$$p_n^{surf} = -\frac{1}{2} \{v_1^*(x_3) \quad 0 \quad v_3^*(x_3)\} \cdot \begin{bmatrix} \bar{T}_{11}^M(x_3) & 0 & \bar{T}_{13}^M(x_3) \\ 0 & 0 & 0 \\ \bar{T}_{31}^M(x_3) & 0 & \bar{T}_{33}^M(x_3) \end{bmatrix} \cdot \begin{Bmatrix} 0 \\ 0 \\ 1 \end{Bmatrix} \Bigg|_{x_3=-h}^{x_3=h}, \quad (19)$$

Additionally, the power flux resulting from the nonlinear body force is given by

$$p_n^{vol} = \frac{1}{2} \int_{-h}^h \{v_1^*(x_3), 0, v_3^*(x_3)\} \cdot \begin{Bmatrix} \bar{f}_1^M(x_3) \\ 0 \\ \bar{f}_3^M(x_3) \end{Bmatrix} dx_3. \quad (20)$$

### 3. Nonzero Power Flux

From Equations (7) and (8), one of the binding conditions that must be satisfied for the mutual interactions is nonzero power flux ( $p_n^{surf} + p_n^{vol} \neq 0$ ) [31]: nonzero power transfer from the selecting primary waves to the modulated waves should be ensured. For this purpose, the power flux from symmetric–symmetric, antisymmetric–antisymmetric, or symmetric–antisymmetric mutual interaction fundamental fields to a prescribed Lamb secondary mode were analyzed in this study to clarify the existence of symmetric or antisymmetric mode due to Lamb wave mutual interactions.

As in Ref. [32], similar generic symmetric and antisymmetric functions ( $S = S(x_3)$  and  $A = A(x_3)$ , respectively) were defined to investigate symmetries along the  $x_3$ -axis.

(1) Symmetric–symmetric or antisymmetric–antisymmetric mutual interactions.

When the two mutually interacting fundamental excitations are the same mode type, the nonlinear forcing terms will have the same symmetry properties as mode self-interaction, as shown in Refs. [21,32]. Thus,

$$\begin{aligned} p_n^{surf} + p_n^{vol} &= 0 \text{ for secondary antisymmetric Lamb waves} \\ p_n^{surf} + p_n^{vol} &\neq 0 \text{ for secondary symmetric Lamb waves} \end{aligned} \quad (21)$$

The results indicate that both a symmetric–symmetric and an antisymmetric–antisymmetric mutual interaction can excite a symmetric type secondary mode. In contrast, neither a symmetric–symmetric nor an antisymmetric–antisymmetric mutual interaction can excite an antisymmetric type secondary mode.

(2) Symmetric–antisymmetric mutual interaction.

Now, let a fundamental mode  $a$  be symmetric Lamb mode and the other fundamental mode  $b$  be antisymmetric Lamb mode, whose displacement field is given in Equations (1) and (3). Thus, the symmetries of the displacement are given by

$$u_1^a = S(x_3), u_3^a = A(x_3), u_1^b = A(x_3), u_3^b = S(x_3) \tag{22}$$

By using these results, the symmetries of  $\mathbf{v}$ ,  $\mathbf{T}$ ,  $\mathbf{f}$  are shown in Table 1.

**Table 1.** The symmetries of velocity and nonlinear forcing terms for different secondary modes from the symmetric–antisymmetric mode mutual interaction.

Secondary Mode Type	$\mathbf{v}$	$\mathbf{T}$	$\mathbf{f}$
Symmetric	{S 0 A}	$\begin{bmatrix} A & 0 & S \\ 0 & 0 & 0 \\ S & 0 & A \end{bmatrix}$	$\begin{Bmatrix} A \\ 0 \\ S \end{Bmatrix}$
Antisymmetric	{A 0 S}	$\begin{bmatrix} A & 0 & S \\ 0 & 0 & 0 \\ S & 0 & A \end{bmatrix}$	$\begin{Bmatrix} A \\ 0 \\ S \end{Bmatrix}$

Hence, for secondary symmetric modes, Equations (19) and (20) become

$$p_n^{vol} = \frac{1}{2} \int_{-h}^h \{S \ 0 \ A\} \cdot \begin{Bmatrix} A \\ 0 \\ S \end{Bmatrix} dx_3 = \frac{1}{2} \int_{-h}^h (S \cdot A + A \cdot S) dx_3 = 0 \tag{23}$$

$$p_n^{surf} = -\frac{1}{2} \{S \ 0 \ A\} \cdot \begin{bmatrix} A & 0 & S \\ 0 & 0 & 0 \\ S & 0 & A \end{bmatrix} \cdot \begin{Bmatrix} 0 \\ 0 \\ 1 \end{Bmatrix} \Big|_{x_3=-h}^{x_3=h} = -\frac{1}{2} (S \cdot S + A \cdot A) \Big|_{x_3=-h}^{x_3=h} = 0 \tag{24}$$

Whereas for secondary antisymmetric modes, we obtain

$$p_n^{vol} = \frac{1}{2} \int_{-h}^h \{A \ 0 \ S\} \cdot \begin{Bmatrix} A \\ 0 \\ S \end{Bmatrix} dx_3 = \frac{1}{2} \int_{-h}^h (A \cdot A + S \cdot S) dx_3 \neq 0 \tag{25}$$

$$p_n^{surf} = -\frac{1}{2} \{A \ 0 \ S\} \cdot \begin{bmatrix} A & 0 & S \\ 0 & 0 & 0 \\ S & 0 & A \end{bmatrix} \cdot \begin{Bmatrix} 0 \\ 0 \\ 1 \end{Bmatrix} \Big|_{x_3=-h}^{x_3=h} = -\frac{1}{2} (A \cdot S + S \cdot A) \Big|_{x_3=-h}^{x_3=h} \neq 0, \tag{26}$$

By summarizing these results, it can be concluded that only symmetric secondary wave fields can be excited for symmetric–symmetric mode mutual interaction or antisymmetric–antisymmetric mode mutual interaction, while only antisymmetric secondary wave fields can be excited for symmetric–antisymmetric mode mutual interaction.

Table 2 lists all the possible secondary wave fields due to Lamb wave mode mutual interactions.

**Table 2.** Possible secondary wave fields due to Lamb wave mode mutual interactions.

Fundamental Wave Field	Secondary Modulation
Symmetric–symmetric	Symmetric
Antisymmetric–antisymmetric	Symmetric
Symmetric–antisymmetric	Antisymmetric

#### 4. Synchronism Condition

Besides nonzero power flux, synchronism (or phase velocity matching) is the other binding condition that must be satisfied for the mutual interactions [31]; that is,  $k_n^* = (k_b \pm k_a)$  when  $f_b > f_a$  is assumed.

A parameter  $k_d$  was employed to evaluate the intensity of phase velocity matching at different primary frequencies pairs, which is given by

$$k_{d\pm}(f_b, f_a) = -\frac{\|k_n^* - (k_b \pm k_a)\|}{\|k_n^*\|}, \quad (27)$$

where  $\|\cdot\|$  is the absolute-value norm;  $f_b, f_a$ , and  $f_n$  are the central frequencies of primary wave  $b, a$ , and modulated wave, respectively. Its value is closer to zero, and the intensity of phase velocity matching is higher.

In this study, the generation of modulated waves from fundamental modes (S0 mode and A0 mode) interactions in an aluminum plate (thickness 3 mm, density 2700 kg/m<sup>3</sup>) were discussed. Only four mode types satisfy the nonzero power flux condition: A0A0-S0, S0S0-S0, S0A0-A0, and A0S0-A0. Here, S0A0-A0 represents the generation of the A0 mode Lamb wave due to the mutual interactions of S0 mode wave  $a$  with low frequency and A0 mode wave  $b$  with high frequency. The intensity of phase velocity matching shows that S0S0-S0 and S0A0-A0 have the potential for a nonlinear modulation test since there are many pairs that satisfy both phase velocity matching and nonzero power flux condition, as shown in Figure 3c–f. Contrarily, A0A0-S0 and A0S0-A0 cannot generate modulated waves since phase velocity matching did not occur at any pairs, as shown in Figure 3.

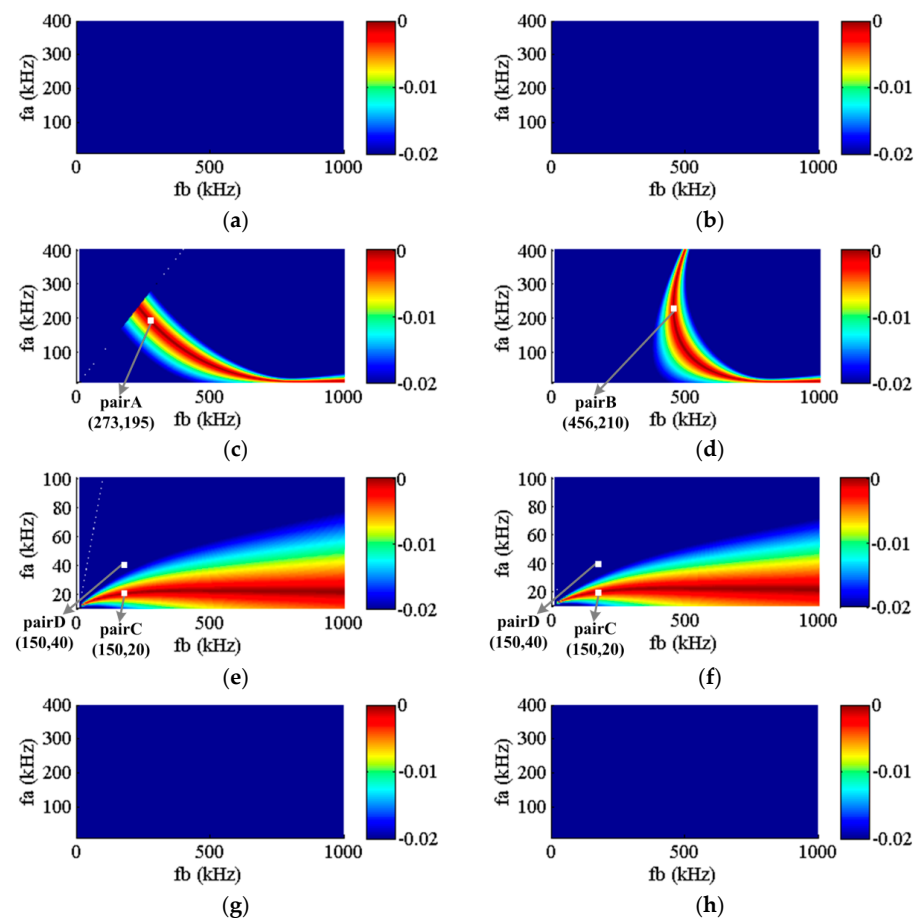


**Figure 3.** The modulation plots of A0A0–S0, S0S0–S0, S0A0–A0, A0S0–A0: (a)  $k_{d+}$  of A0A0–S0; (b)  $k_{d-}$  of A0A0–S0; (c)  $k_{d+}$  of S0S0–S0; (d)  $k_{d-}$  of S0S0–S0; (e)  $k_{d+}$  of S0A0–A0; (f)  $k_{d-}$  of S0A0–A0; (g)  $k_{d+}$  of A0S0–A0; (h)  $k_{d-}$  of A0S0–A0.

## 5. Experimental Research

### 5.1. Experimental Setup

An experiment was carried out on a 3 mm thick 6061-T6 aluminum plate to test the theoretical result. A fatigue crack was introduced to the specimen by applying a sinusoidal tensile load of 10 Hz using a fatigue testing machine SDS200. It took about 160,000 cycles to produce a 30 mm long fatigue crack from the hole at the center of the specimen, as shown in Figure 4.

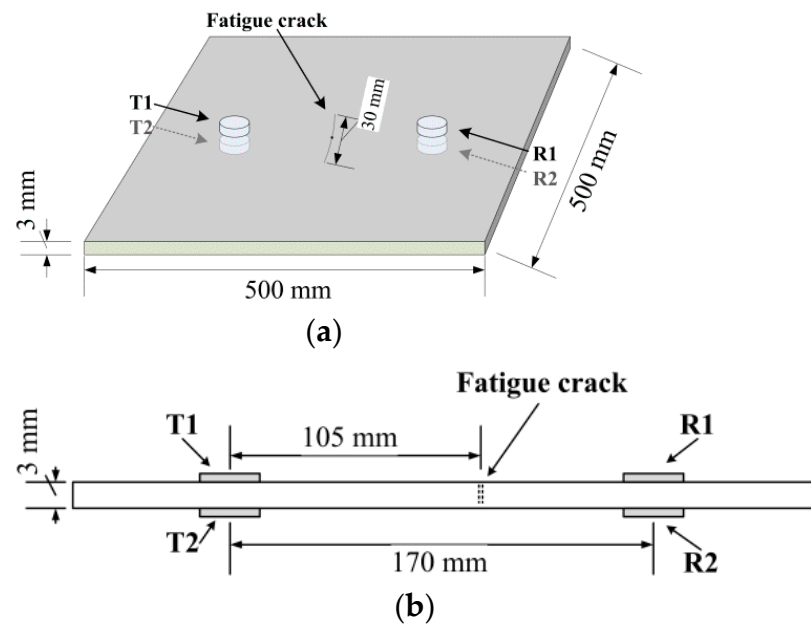


**Figure 4.** Schematic diagram of the experimental setup: (a) top view (b) front view.

Four identical piezoelectric discs (APC 851) were installed on the specimen, whose diameter and thickness was 6.6 mm and 0.24 mm, respectively. A dual-PZT scheme was applied to generate and receive selective symmetric and antisymmetric modes.

The summation of two sinusoidal tone-burst signals enclosed in a Hanning window at a central frequency of the low and the high frequencies with a 1 ms duration were applied as input.

The input signal was generated by an arbitrary waveform generation unit (Agilent® 33220A, Santa Clara, CA, USA), then it was amplified to 45 (V) using a linear amplifier (T&C power conversion, Inc. AG series, Rochester, NY, USA) to drive the PZT actuators. Wave signals were captured using an oscilloscope (Agilent® DSO5032A, Santa Clara, CA, USA) at a sampling rate of 10 MHz with 25 times averaging. Then the measured signals were analyzed in the frequency domain by applying a short-time Fourier transform (STFT) up to the first arrival wave packet.

### 5.2. Experimental Results

Four pairs (pair A~D) of primary mode were chosen for the demonstration shown in Figure 3. Details for these pairs are given in Table 3. For the S0S0-S0 type, the synchronism condition was matched at pair A, and the modulation frequency was  $195 + 273 = 468$  kHz, as well as pair B with modulation frequency  $456 - 210 = 246$  kHz. As shown in Figure 5, the S0 mode modulation is generated at 468 kHz from 195 kHz S0 and 273 kHz S0 mode primary waves only when the nonzero power flux and synchronism condition are matched. In the same way, the S0 mode modulation was generated at 246 kHz when both primary waves at 210 kHz and 456 kHz were S0 mode, as shown in Figure 6.

**Table 3.** Four pairs of primary mode for the demonstration.

No.	Waves	Primary Mode	Frequency	Synchronism	Theoretical Modulation
1	<i>a</i> <i>b</i>	S0 S0	195 kHz 273 kHz	Only for $f_b + f_a$	S0 mode at 468 kHz
2	<i>a</i> <i>b</i>	S0 S0	210 kHz 456 kHz	Only for $f_b - f_a$	S0 mode at 246 kHz
3	<i>a</i> <i>b</i>	A0 S0	20 kHz 150 kHz	Both $f_b + f_a$ and $f_b - f_a$	A0 mode at 170 kHz and 130 kHz
4	<i>a</i> <i>b</i>	A0 S0	40 kHz 150 kHz	None	None

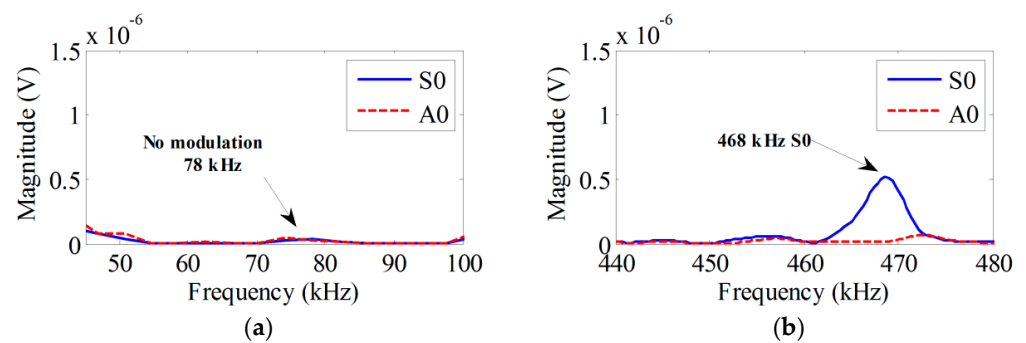


**Figure 5.** The S0 mode modulation is generated at 468 kHz only when the nonzero power flux and synchronism condition are matched (both primary waves at 195 kHz and 273 kHz are S0 mode): (a) No modulation at 78 kHz; (b) S0 at 468 kHz.

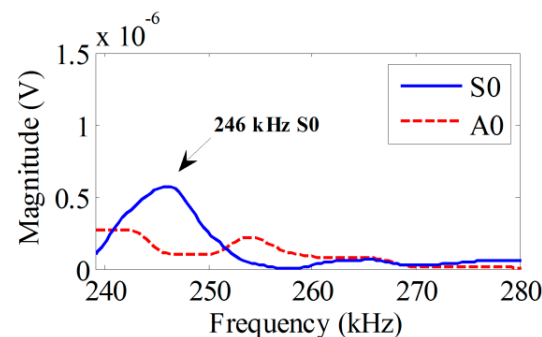


**Figure 6.** The S0 mode modulation is generated at 246 kHz only when the nonzero power flux and synchronism condition are matched (both primary waves at 210 kHz and 456 kHz are S0 mode).

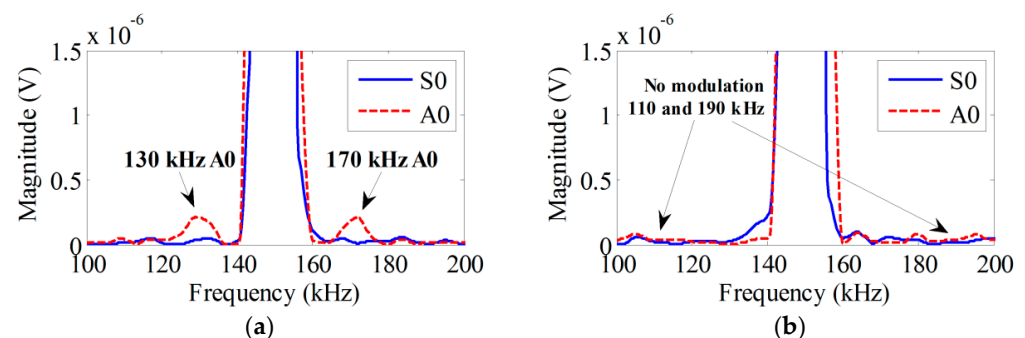


**Figure 7.** The A0 mode modulation is generated at both 130 kHz and 170 kHz from 20 kHz A0 mode and 150 kHz S0 mode, as shown in (a), while no modulation is generated from 40 kHz A0 mode and 150 kHz S0 mode when the synchronism condition is not matched as shown in (b): (a) S0 at 130 kHz and 170 kHz; (b) A0 at 130 kHz and 170 kHz.

For the S0A0-A0 type, the synchronism condition was matched at pair C, and the modulation frequencies are  $150 \pm 20$  kHz. Therefore, The A0 mode modulation is generated at both 130 kHz and 170 kHz, as shown in Figure 7a. On the other hand, the synchronism condition was not satisfied when  $f_a$  was shifted to 40 kHz at pair D; therefore, no modulation was generated, as shown in Figure 7b.

## 6. Conclusions

In summary, it was demonstrated that only symmetric secondary wave fields could be generated by symmetric–symmetric or antisymmetric–antisymmetric mode mutual interactions, while only antisymmetric secondary wave fields can be generated by symmetric–antisymmetric mode mutual interactions. The theory of Lamb wave mutual interaction can be utilized to guide nonlinear mode selection with a frequency range under 520 kHz. The fatigue damage in the metal plate can be detected by the Lamb wave mutual interaction. The theoretical results agree with that of cumulative harmonic generation [4,32]; therefore, it was shown that the interactions (both self-interactions and mutual interactions) of two Lamb modes of the same nature (symmetric or antisymmetric) leads to secondary wave fields that are symmetric modes, while interactions between two modes of opposite nature lead to secondary wave fields that are antisymmetric modes.

The ability to effectively select primary pairs is also demonstrated by experimental results. These results are important for the development of nonlinear modulation technology in nondestructive evaluation (NDE) and structural health monitoring (SHM) applications.

**Author Contributions:** Theoretical derivation, S.M.; performing and designing the experiments, G.Z. and L.W.; writing—original draft preparation, S.M. and G.Z.; writing—review and editing, L.W. and H.H.; supervision and funding acquisition, S.M. and H.H. All authors have read and agreed to the published version of the manuscript.

**Funding:** Natural Science Foundation of Liaoning Province of China (No. 2022-MS-422). Science and technology research project of Liaoning Provincial Department of Education (No. L2020005, No. LJKMZ20221908).

**Data Availability Statement:** Not applicable.

**Acknowledgments:** The authors acknowledge the financial support from Natural Science Foundation of Liaoning Province of China: 2022-MS-422; Science and technology research project of the Liaoning Provincial Department of Education: L2020005, LJKMZ20221908.

**Conflicts of Interest:** The authors declare no conflict of interest.

## Appendix A

### Appendix A.1 Nonlinear Forcing Terms

The nonlinear forcing terms for the mode mutual interactions of two Lamb modes can be obtained via Equations (15) and (16) by considering  $u_2 = 0$  and requiring  $u_i$  to be independent of  $x_2$ . The nonzero terms of the nonlinear part of the first Piola–Kirchhoff stress for the mode mutual interactions of two Lamb mode fundamental wave fields are given by

$$\begin{aligned} \bar{T}_{11}^M = & (3\lambda + 6\mu + 2C + 6B + 2A) \frac{\partial u_1^a}{\partial x_1} \frac{\partial u_1^b}{\partial x_1} + \left( \mu + B + \frac{A}{2} \right) \left( \frac{\partial u_1^a}{\partial x_3} \frac{\partial u_3^b}{\partial x_1} + \frac{\partial u_3^a}{\partial x_1} \frac{\partial u_1^b}{\partial x_3} \right) \\ & + (\lambda + 2C + 2B) \left( \frac{\partial u_3^a}{\partial x_3} \frac{\partial u_3^b}{\partial x_3} + \frac{\partial u_1^a}{\partial x_1} \frac{\partial u_3^b}{\partial x_3} + \frac{\partial u_3^a}{\partial x_3} \frac{\partial u_1^b}{\partial x_1} \right) \\ & + \left( \lambda + 2\mu + B + \frac{A}{2} \right) \left( \frac{\partial u_1^a}{\partial x_3} \frac{\partial u_1^b}{\partial x_3} + \frac{\partial u_3^a}{\partial x_1} \frac{\partial u_3^b}{\partial x_1} \right), \end{aligned} \quad (A1)$$

$$\begin{aligned} \bar{T}_{13}^M = & \left( \mu + B + \frac{A}{2} \right) \left( \frac{\partial u_3^a}{\partial x_3} \frac{\partial u_1^b}{\partial x_3} + \frac{\partial u_1^a}{\partial x_3} \frac{\partial u_3^b}{\partial x_3} + \frac{\partial u_1^a}{\partial x_3} \frac{\partial u_1^b}{\partial x_1} + \frac{\partial u_1^a}{\partial x_1} \frac{\partial u_1^b}{\partial x_3} \right) \\ & + \left( \lambda + 2\mu + B + \frac{A}{2} \right) \left( \frac{\partial u_3^a}{\partial x_1} \frac{\partial u_3^b}{\partial x_3} + \frac{\partial u_3^a}{\partial x_3} \frac{\partial u_3^b}{\partial x_1} + \frac{\partial u_3^a}{\partial x_1} \frac{\partial u_1^b}{\partial x_1} + \frac{\partial u_1^a}{\partial x_1} \frac{\partial u_3^b}{\partial x_1} \right), \end{aligned} \quad (A2)$$

$$\begin{aligned} \bar{T}_{31}^M = & \left( \mu + B + \frac{A}{2} \right) \left( \frac{\partial u_3^a}{\partial x_3} \frac{\partial u_3^b}{\partial x_1} + \frac{\partial u_3^a}{\partial x_1} \frac{\partial u_3^b}{\partial x_3} + \frac{\partial u_3^a}{\partial x_1} \frac{\partial u_1^b}{\partial x_1} + \frac{\partial u_1^a}{\partial x_1} \frac{\partial u_3^b}{\partial x_1} \right) \\ & + \left( \lambda + 2\mu + B + \frac{A}{2} \right) \left( \frac{\partial u_3^a}{\partial x_3} \frac{\partial u_1^b}{\partial x_3} + \frac{\partial u_1^a}{\partial x_3} \frac{\partial u_3^b}{\partial x_3} + \frac{\partial u_1^a}{\partial x_3} \frac{\partial u_1^b}{\partial x_1} + \frac{\partial u_1^a}{\partial x_1} \frac{\partial u_3^b}{\partial x_3} \right), \end{aligned} \quad (A3)$$

$$\begin{aligned} \bar{T}_{33}^M = & (3\lambda + 6\mu + 2C + 6B + 2A) \frac{\partial u_3^a}{\partial x_3} \frac{\partial u_3^b}{\partial x_3} + \left( \mu + B + \frac{A}{2} \right) \left( \frac{\partial u_1^a}{\partial x_3} \frac{\partial u_3^b}{\partial x_1} + \frac{\partial u_3^a}{\partial x_1} \frac{\partial u_1^b}{\partial x_3} \right) \\ & + (\lambda + 2C + 2B) \left( \frac{\partial u_1^a}{\partial x_1} \frac{\partial u_1^b}{\partial x_1} + \frac{\partial u_1^a}{\partial x_1} \frac{\partial u_3^b}{\partial x_3} + \frac{\partial u_3^a}{\partial x_3} \frac{\partial u_1^b}{\partial x_1} \right) \\ & + \left( \lambda + 2\mu + B + \frac{A}{2} \right) \left( \frac{\partial u_1^a}{\partial x_3} \frac{\partial u_1^b}{\partial x_3} + \frac{\partial u_3^a}{\partial x_1} \frac{\partial u_3^b}{\partial x_1} \right). \end{aligned} \quad (A4)$$

## References

- Li, W.; Xiao, J.; Deng, M. Micro-defect imaging with an improved resolution using nonlinear ultrasonic Lamb waves. *J. Appl. Phys.* **2022**, *131*, 185101. [\[CrossRef\]](#)
- Li, W.; Lan, Z.; Hu, N.; Deng, M. Modeling and simulation of backward combined harmonic generation induced by one-way mixing of longitudinal ultrasonic guided waves in a circular pipe. *Ultrasonics* **2021**, *113*, 106356. [\[CrossRef\]](#) [\[PubMed\]](#)
- Li, W.; Lan, Z.; Hu, N.; Deng, M. Theoretical and numerical investigations of the nonlinear acoustic response of feature guided waves in a welded joint. *Wave Motion* **2021**, *101*, 102696. [\[CrossRef\]](#)
- Krishna Chillara, V.; Lissenden, C.J. Interaction of guided wave modes in isotropic weakly nonlinear elastic plates: Higher harmonic generation. *J. Appl. Phys.* **2012**, *111*, 124909. [\[CrossRef\]](#)
- Zhao, J.; Chillara, V.K.; Ren, B.; Cho, H.; Qiu, J.; Lissenden, C.J. Second harmonic generation in composites: Theoretical and numerical analyses. *J. Appl. Phys.* **2016**, *119*, 064902. [\[CrossRef\]](#)
- Liu, Y.; Chillara, V.K.; Lissenden, C.J.; Rose, J.L. Third harmonic shear horizontal and Rayleigh Lamb waves in weakly nonlinear plates. *J. Appl. Phys.* **2013**, *114*, 195. [\[CrossRef\]](#)
- Duan, W.; Niu, X.; Gan, T.-H.; Kanfoud, J.; Chen, H.-P. A numerical study on the excitation of guided waves in rectangular plates using multiple point sources. *Metals* **2017**, *7*, 552. [\[CrossRef\]](#)
- Jankauskas, A.; Mazeika, L. Ultrasonic guided wave propagation through welded lap joints. *Metals* **2016**, *6*, 315. [\[CrossRef\]](#)
- Draudvilienė, L.; Meškuotienė, A. The methodology for the reliability evaluation of the signal processing methods used for the dispersion estimation of Lamb waves. *IEEE Trans. Instrum. Meas.* **2021**, *71*, 1–7. [\[CrossRef\]](#)
- Draudvilienė, L.; Tumsys, O.; Mazeika, L.; Zukauskas, E. Estimation of the Lamb wave phase velocity dispersion curves using only two adjacent signals. *Compos. Struct.* **2021**, *258*, 113174. [\[CrossRef\]](#)
- Sohn, H.; Lim, H.J.; DeSimio, M.P.; Brown, K.; Derriso, M. Nonlinear ultrasonic wave modulation for online fatigue crack detection. *J. Sound Vib.* **2014**, *333*, 1473–1484. [\[CrossRef\]](#)
- Solodov, I.; Busse, G. Nonlinear air-coupled emission: The signature to reveal and image microdamage in solid materials. *Appl. Phys. Lett.* **2007**, *91*, 251910. [\[CrossRef\]](#)
- Jhang, K.-Y. Nonlinear ultrasonic techniques for nondestructive assessment of micro damage in material: A review. *Int. J. Precis. Eng. Manuf.* **2009**, *10*, 123–135. [\[CrossRef\]](#)
- Liu, Y.; Khajeh, E.; Lissenden, C.J.; Rose, J.L. Interaction of torsional and longitudinal guided waves in weakly nonlinear circular cylinders. *J. Acoust. Soc. Am.* **2013**, *133*, 2541–2553. [\[CrossRef\]](#)
- Cho, H.; Hasanian, M.; Shan, S.; Lissenden, C.J. Nonlinear guided wave technique for localized damage detection in plates with surface-bonded sensors to receive Lamb waves generated by shear-horizontal wave mixing. *NDT E Int.* **2019**, *102*, 35–46. [\[CrossRef\]](#)
- Shen, Y.; Wang, J.; Xu, W. Nonlinear features of guided wave scattering from rivet hole nucleated fatigue cracks considering the rough contact surface condition. *Smart Mater. Struct.* **2018**, *27*, 105044. [\[CrossRef\]](#)
- Shan, S.; Hasanian, M.; Cho, H.; Lissenden, C.J.; Cheng, L. New nonlinear ultrasonic method for material characterization: Codirectional shear horizontal guided wave mixing in plate. *Ultrasonics* **2019**, *96*, 64–74. [\[CrossRef\]](#)
- Hong; Ming; Zhongqing; Mao; Zhu; Todd; Michael, D. Uncertainty quantification for acoustic nonlinearity parameter in Lamb wave-based prediction of barely visible impact damage in composites. *Mech. Syst. Signal Process.* **2017**, *82*, 448–460. [\[CrossRef\]](#)
- Pineda Allen, J.C.; Ng, C.T. Nonlinear guided-wave mixing for condition monitoring of bolted joints. *Sensors* **2021**, *21*, 5093. [\[CrossRef\]](#)
- Aseem, A.; Ng, C.T. Debonding detection in rebar-reinforced concrete structures using second harmonic generation of longitudinal guided wave. *Ndt E Int.* **2021**, *122*, 102496. [\[CrossRef\]](#)
- Liu, Y.; Chillara, V.K.; Lissenden, C.J. On selection of primary modes for generation of strong internally resonant second harmonics in plate. *J. Sound Vib.* **2013**, *332*, 4517–4528. [\[CrossRef\]](#)
- Jin Lim, H.; Sohn, H.; Liu, P. Binding conditions for nonlinear ultrasonic generation unifying wave propagation and vibration. *Appl. Phys. Lett.* **2014**, *104*, 214103. [\[CrossRef\]](#)
- Kim, Y.; Lim, H.J.; Sohn, H. Nonlinear ultrasonic modulation based failure warning for aluminum plates subject to fatigue loading. *Int. J. Fatigue* **2018**, *114*, 130–137. [\[CrossRef\]](#)

24. Lim, H.J.; Sohn, H.; Kim, Y. Data-driven fatigue crack quantification and prognosis using nonlinear ultrasonic modulation. *Mech. Syst. Signal Process.* **2018**, *109*, 185–195. [[CrossRef](#)]
25. Ding, X.; Xu, C.; Deng, M.; Zhao, Y.; Bi, X.; Hu, N. Experimental investigation of the surface corrosion damage in plates based on nonlinear Lamb wave methods. *Ndt E Int.* **2021**, *121*, 102466. [[CrossRef](#)]
26. Cirtautas, D.; Samaitis, V.; Mažeika, L.; Raišutis, R.; Žukauskas, E. Selection of Higher Order Lamb Wave Mode for Assessment of Pipeline Corrosion. *Metals* **2022**, *12*, 503. [[CrossRef](#)]
27. Kim, J.; Park, J.; Zhu, B.; Cho, Y. Nonlinear Ultrasonic Guided Wave Method Using Semi-Analytical Finite Element (SAFE) Technique on a Damaged SWO-V Spring Coil. *Metals* **2021**, *11*, 752. [[CrossRef](#)]
28. Graff, K.F. *Wave Motion in Elastic Solids*; Dover Publications: New York, NY, USA, 1975.
29. Matsuda, N.; Biwa, S. Phase and group velocity matching for cumulative harmonic generation in Lamb waves. *J. Appl. Phys.* **2011**, *109*, 094903. [[CrossRef](#)]
30. Auld, B.A. *Acoustic Fields and Waves in Solids*, 2nd ed.; Krieger Publishing Company: Malabar, FL, USA, 1990.
31. De Lima, W.; Hamilton, M. Finite-amplitude waves in isotropic elastic plates. *J. Sound Vib.* **2003**, *265*, 819–839. [[CrossRef](#)]
32. Müller, M.F.; Kim, J.-Y.; Qu, J.; Jacobs, L.J. Characteristics of second harmonic generation of Lamb waves in nonlinear elastic plates. *J. Acoust. Soc. Am.* **2010**, *127*, 2141–2152. [[CrossRef](#)]